Letter

Prediction of ferroelectric superconductors with reversible superconducting diode effect

Baxing Zhai [1], Bohao Li [1], Yao Wen [1], Fengcheng Wu [1,2,*] and Jun He [1,2,†]

[1] *Key Laboratory of Artificial Micro and Nanostructures of Ministry of Education, and School of Physics and Technology, Wuhan University, Wuhan 430072, China*

[2] *Wuhan Institute of Quantum Technology, Wuhan 430206, China*

(Received 5 January 2022; revised 7 October 2022; accepted 11 October 2022; published 24 October 2022)

A noncentrosymmetric superconductor can have a superconducting diode effect, where the critical current in opposite directions is different when time-reversal symmetry is also broken. We theoretically propose that a ferroelectric superconductor with coexisting ferroelectricity and superconductivity can support a ferroelectric reversible superconducting diode effect. Through first-principles calculation, we predict that monolayer $CuNb_2Se_4$ (i.e., bilayer $NbSe_2$ intercalated with Cu) is such a ferroelectric superconductor, where ferroelectricity controls the layer polarization as well as the sign of spin-orbit-coupling-induced spin splittings. Because the nonreciprocal effect of the critical current is proportional to the spin splittings, the superconducting diode effect is reversible upon electric switch of ferroelectricity. While we use $CuNb_2Se_4$ as a model system, the predicted effect can appear in a class of two-dimensional superconducting bilayers with ferroelectricity induced by interlayer sliding. Our work opens the door to studying the interplay between superconductivity and ferroelectricity in two-dimensional materials.

DOI: 10.1103/PhysRevB.106.L140505

Introduction. A noncentrosymmetric material can support nonreciprocal charge transport, where the electrical resistance becomes different if the direction of the charge current is reversed. Recently, nonreciprocal phenomena in superconductors have become an active research topic [1–18]. In bulk metals without the inversion symmetry, nonreciprocal charge transport occurs when the time-reversal symmetry is also broken. This nonreciprocity induced by the magnetochiral anisotropy is significantly enhanced for the paraconductivity near the superconducting transition temperature T_c because of the superconducting fluctuation [1]. Moreover, in the superconducting state below T_c, the critical current along opposite directions differs, i.e., $j_c(\hat{n}) \neq j_c(-\hat{n})$, where $j_c(\hat{n})$ represents the magnitude of the critical current along direction $\hat{n}$. This nonreciprocity results in the superconducting diode effect (SDE) [7], where the system is superconducting in one direction but resistive in the opposite direction if the applied current has a magnitude between $j_c(\hat{n})$ and $j_c(-\hat{n})$. The SDE was recently observed experimentally in several systems [7–12,19], including an artificial superlattice $[Nb/V/Ta]_n$ [7] and a heterostructure of the twisted trilayer graphene and WSe_2 [19]. Theory on the SDE was developed based on Ginzburg-Landau free energy as well as microscopic calculation [14–18].

In this Letter, we introduce a new type of noncentrosymmetric superconductors, i.e., ferroelectric superconductors, where ferroelectricity acts as a new knob in tuning superconductivity. A ferroelectric material breaks the inversion symmetry with a spontaneous electric polarization that can be reversed by an applied electric field. While ferroelectric semiconductors/insulators have been widely studied, ferroelectricity can also exist in metals as exemplified by few-layer WTe_2 [20]. When a ferroelectric metal (also known as polar metal) becomes superconducting at low temperatures, a ferroelectric superconductor forms and supports the SDE if time-reversal symmetry is further broken. We predict that the superconducting direction of the diode can be reversed upon ferroelectric reversal, which we term as the reversible SDE. This prediction represents an example on the controlling of superconductivity through ferroelectricity.

For material realization, we propose monolayer $CuNb_2Se_4$ to be a ferroelectric superconductor with the reversible SDE. Monolayer $CuNb_2Se_4$ can be viewed as a 2H bilayer $NbSe_2$ intercalated by Cu atoms, as illustrated in Fig. 1. We establish both ferroelectricity and superconductivity in this material through first-principles calculations. The ferroelectricity in monolayer $CuNb_2Se_4$ controls the layer and spin degrees of freedom of low-energy states across the Fermi energy in $\pm K$ valleys (two corners of the hexagonal Brillouin zone), where both the layer polarization and the valley-dependent spin splittings [induced by spin-orbit coupling (SOC)] are reversed by ferroelectric reversal. In the superconducting state, the nonreciprocal factor η [Eq. (8)] of the critical current is proportional to the SOC-induced spin splittings. Therefore, η changes sign by the reverse of ferroelectricity, which leads to the reversible SDE. While we study monolayer $CuNb_2Se_4$ in detail to elucidate the physics, reversible SDE is generally expected in ferroelectric superconductors, which can be realized in van der Waals (vdW) superconducting bilayers with ferroelectricity arising from interlayer sliding [21]. Our work not only presents a novel approach to detect ferroelectricity

*wufcheng@whu.edu.cn
†he-jun@whu.edu.cn

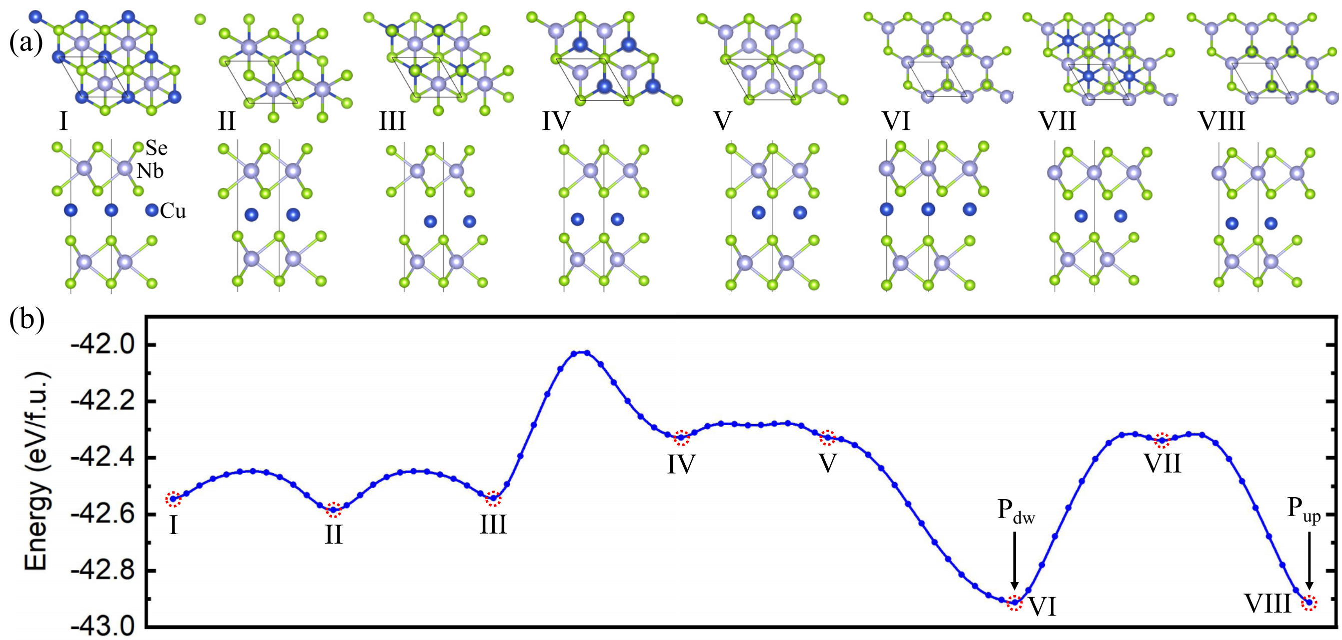

FIG. 1. (a) Top and side views of eight high-symmetry structures of monolayer $CuNb_2Se_4$. In structures I to III, Nb atoms are aligned vertically. In structures IV and V, Se atoms are aligned vertically. In structures VI to VIII, Nb atoms are aligned with Se atoms vertically. Structures II and VII are inversion symmetric, while other structures are not. (b) The energy per formula unit for different lattice structures of monolayer $CuNb_2Se_4$. The red dashed circles mark the high-symmetry structures shown in (a). The transition structures between two neighboring high-symmetry structures are generated by the nudged-elastic band method.

through superconducting transport, but also opens up new opportunities for the construction of electrically controllable and nondissipative diodes.

Ferroelectricity. The vdW materials, such as graphite and transition metal dichalcogenides (e.g., NbS_2, $NbSe_2$, MoS_2), can be the intercalation host, which provides a powerful approach to induce a variety of exotic quantum phenomena [22–28] including ferroelectricity [29]. Intercalation has also been achieved in the two-dimensional (2D) limit [30–32]. Here we theoretically study monolayer $CuNb_2Se_4$. The strategy is to start from a prototypical 2D superconductor (i.e., bilayer $NbSe_2$) [33], which we show to develop ferroelectricity upon Cu intercalation while remaining superconducting.

We demonstrate ferroelectricity in monolayer $CuNb_2Se_4$ by studying eight high-symmetry structures, as illustrated in Fig. 1(a). In the monolayer $CuNb_2Se_4$ under study, the top and bottom $NbSe_2$ layers are rotated by 180°. The eight structures can be distinguished by the in-plane relative positions of the top $NbSe_2$ layer, the middle Cu layer and the bottom $NbSe_2$ layer. We perform lattice relaxation for each structure using first-principles calculation implemented in the Vienna *ab initio* simulation package (VASP) [34] and obtain the corresponding energy. The energy landscape plotted in Fig. 1(b) shows that two different structures, i.e., structures VI and VIII, have the same lowest energy. We note that VI and VIII structures are inversion partners, although each of them on its own lacks inversion symmetry. Therefore, the VI and VIII structures have the same energy, but opposite layer polarizations, which gives rise to ferroelectricity. We further perform *ab initio* molecular dynamics (AIMD) simulations and phonon spectrum calculations for these two structures to verify structural stability. The computational details are presented in the Supplemental Material (SM) [35] (see, also, Refs. [36–39] therein). In AIMD simulations, the energy fluctuates slightly and the structure maintains integrity after 5 ps at 300 K, indicating the thermodynamic stability. Meanwhile, the phonon dispersion calculated using the PHONOPY code [40] has no virtual frequency in the whole Brillouin zone, implying the dynamic stability.

We use Bader charge analysis [41] to quantitatively characterize the ferroelectricity. For structure VI, we find that the average number of electrons transferred from one Cu atom to the top and bottom $NbSe_2$ layers is 0.23 and 0.1, respectively [35], which are unequal because the Cu atoms occupy noncentrosymmetric sites. Thus, the structure VI posses a downward electric dipole moment. By contrast, the structure VIII has an upward electric dipole moment. Hereafter, we refer to VI and VIII structures as P_{dw} and P_{up} structures, respectively. We also confirm the electric polarization by calculating the electrostatic potential difference across the monolayer, as discussed in the SM [35]. We investigate the ferroelectric transition process using the nudged-elastic band method [42]. The transition barrier [Fig. 1(b)] between P_{dw} and P_{up} is about 0.6 eV per formula unit, which is comparable to that of monolayer In_2Se_3 [43]. Therefore, ferroelectric reversal by an applied out-of-plane electric field is feasible in monolayer $CuNb_2Se_4$.

Band Structure. The band structures including SOC effects are plotted in Fig. 2. Because P_{up} and P_{dw} structures are inversion partners and time-reversal symmetry is preserved, their band structures have identical energy dispersion. At the Fermi energy, there are eight Fermi pockets, of which four are in the Γ valley, two in the $+K$ valley, and two in the $-K$ valley

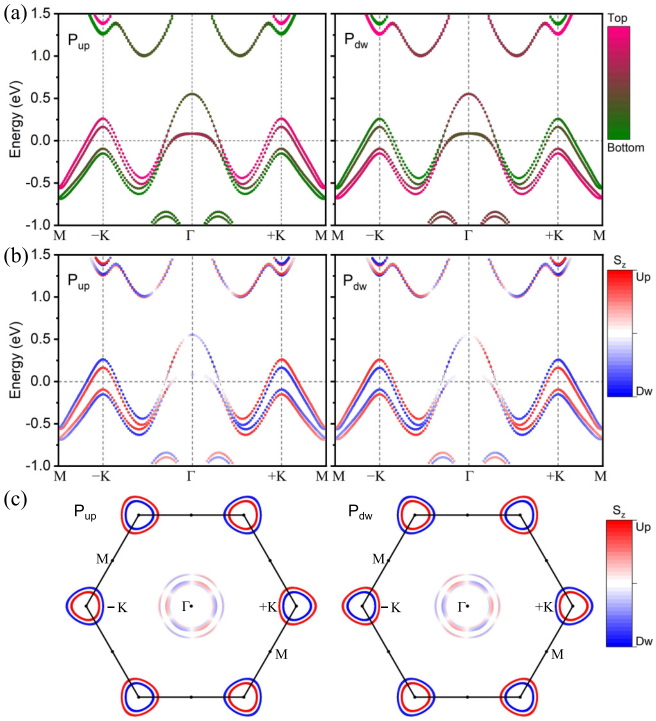

FIG. 2. (a) The layer-projected band structure of monolayer $CuNb_2Se_4$ with SOC effect for P_{up} (left panel) and P_{dw} (right panel). (b) The spin-projected band structure. The spin projection is along out-of-plane $\hat{z}$ axis with red representing spin up and blue representing spin down. Fermi energy is set to be 0 in (a) and (b). (c) The spin-projected Fermi surfaces.

[Fig. 2(c)]. Here Γ and $\pm K$ represent, respectively, the center and two inequivalent corners of the Brillouin zone.

The opposite electric polarization in P_{up} and P_{dw} structures results in differences in electronic states regarding the layer and spin degrees of freedom. The layer-projected band structures in Fig. 2(a) show that the two bands crossing the Fermi energy E_F in $\pm K$ valleys are mainly localized in the top (bottom) $NbSe_2$ layer for the P_{up} (P_{dw}) structure. The opposite layer polarization in combination with the 180° rotation between the two layers leads to ferroelectric reversible spin-valley coupling. To elaborate on this feature, we first focus on the P_{up} structure. In P_{up}, the higher and lower energy bands across E_F carry, respectively, up and down spin polarization in the $+K$ valley, but down and up spin polarization in the $-K$ valley dictated by time-reversal symmetry [Fig. 2(b)]. Here the spin polarization is along the out-of-plane $\hat{z}$ axis. This is the well-known valley-dependent spin splitting effect in transition metal dichalcogenides [44]. We now turn to the P_{dw} structure, where the spin splitting in a given valley is opposite compared to that in the P_{up} structure. Therefore, the spin-valley coupling is controlled by the layer polarization, which is, in turn, controlled by the ferroelectricity.

The spin- and valley-dependent band structure in the $\pm K$ valleys can be described by the following effective Hamiltonian:

$$\mathcal{H}_0 = -\frac{\hbar^2 \boldsymbol{k}^2}{2m^*} + \lambda_w (k_x^3 - 3k_x k_y^2)\tau_z + \Delta_{\mathrm{SOC}}^{(\ell)} \tau_z \sigma_z - E_F, \quad (1)$$

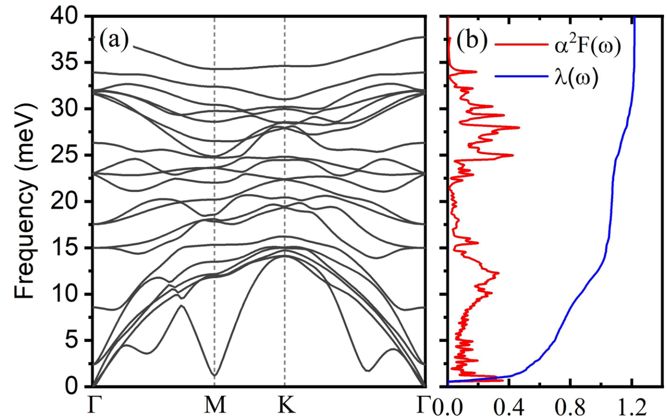

FIG. 3. (a) Phonon dispersion of the monolayer $CuNb_2Se_4$ in P_{up} (P_{dw}) structure. (b) Eliashberg function $\alpha^2F(\omega)$ (red line) and cumulative electron-phonon interaction strength $\lambda(\omega)$ (blue line).

where $\tau_z = \pm$ for $\pm K$ valleys, $\sigma_z = \pm$ for spin up (↑) and down (↓), $\boldsymbol{k} = (k_x, k_y)$ is the momentum defined relative to the $\tau_z K$ point, m^* is the effective mass, λ_w is the parameter of the trigonal warping of the Fermi surfaces, and $\Delta_{\mathrm{SOC}}^{(\ell)}$ is the spin splitting. To capture the dependence on layer polarization, we take $\Delta_{\mathrm{SOC}}^{(\ell)} = \ell \Delta_{\mathrm{SOC}}$ where $\ell = +1$ in the P_{up} structure and $\ell = -1$ in the P_{dw} structure. By fitting to the band structure, we obtain $m^* \approx 0.46 m_0$, $\lambda_w \approx 7.5\ \mathrm{meV \cdot nm^3}$, $\Delta_{\mathrm{SOC}} \approx 50\,\mathrm{meV}$, and $E_F \approx -0.2\,\mathrm{eV}$, where m_0 is the free electron mass. The SOC-induced spin splitting is much weaker in the Γ valley, which we do not analyze in detail.

Superconductivity. Since monolayer $CuNb_2Se_4$ is metallic, it can become superconducting at low temperatures. We note that the intercalation of Cu atoms into *bulk* NbS_2 [45] and $NbSe_2$ [46] was achieved experimentally, and superconductivity persists after the intercalation. Here we consider phonon-mediated superconductivity for the monolayer in the P_{up} (P_{dw}) structure and estimate its superconducting transition temperature T_c based on the McMillan-Allen-Dynes formula [47,48]

$$k_B T_c = \frac{\hbar\omega_{\log}}{1.2} \exp\left(-\frac{1.04(1+\lambda)}{\lambda - \mu^*(1+0.62\lambda)}\right), \quad (2)$$

where

$$\omega_{\log} = \exp\left(\frac{2}{\lambda}\int_0^\infty d\omega \frac{\alpha^2F(\omega)}{\omega}\log\omega\right),$$
$$\lambda = 2\int_0^\infty \frac{\alpha^2F(\omega)}{\omega} d\omega. \quad (3)$$

Here ω is the phonon frequency, $\omega_{\log}$ is the logarithmic average of the phonon frequencies, $\alpha^2F(\omega)$ is the Eliashberg function [49], λ is the electron-phonon coupling strength, and μ^* is the parameter accounting for the Coulomb repulsion. We recalculate the phonon spectra using the density functional perturbation theory (DFPT) as coded in QUANTUM ESPRESSO [50]. The obtained phonon dispersion shown in Fig. 3(a) is consistent with that calculated by the PHONOPY code. The electron-phonon coupling is then calculated using "Electron-phonon Wannier" (EPW) code [51,52], and the results are presented in Fig. 3(b), where λ is found to be 1.22. Taking the empirical parameter μ^* to be 0.15 [49], we obtain a T_c of 3.04 K. This estimation is consistent with the experimental T_c measured in electron-doped bilayer $NbSe_2$ [53], which provides a strong support for our prediction of superconductivity in monolayer $CuNb_2Se_4$.

Superconducting diode effect. A ferroelectric superconductor lacks spatial inversion symmetry and supports SDE provided that time-reversal symmetry $\hat{\mathcal{T}}$ is also broken. To break the $\hat{\mathcal{T}}$ symmetry, we consider a minimal model with a spin-splitting term added to the Hamiltonian, $\mathcal{H} = \mathcal{H}_0 + \Delta_z\sigma_z$, where $\mathcal{H}_0$ is given by Eq. (1). The $\Delta_z\sigma_z$ term can be induced by the proximity effect of a ferromagnetic insulator [54–57]. Here we take Δ_z as a phenomenological parameter to demonstrate the effect. A magnetic-field-free superconducting diode effect was recently demonstrated in Ref. [56], where the time-reversal symmetry breaking for superconductors is generated through proximitized magnetization. This experiment [56] supports our proposal of using proximitized magnetization to induce the superconducting diode effect.

To theoretically analyze the SDE, we focus on states in the $\pm K$ valleys, which have strong SOC-induced spin splittings and contribute most significantly to the SDE. We introduce an order parameter $\Delta_{\boldsymbol{q},\tau_z}$ for intralayer pairing between $(\tau_z, \uparrow)$ and $(-\tau_z, \downarrow)$ states, and $\boldsymbol{q}$ is the center-of-mass momentum of the Cooper pair. The free energy per area for $\Delta_{\boldsymbol{q},\tau_z}$, derived in the SM [35] is given by

$$\begin{aligned}
\mathcal{F}[\Delta_{\boldsymbol{q},\tau_z}] &= \alpha_{\boldsymbol{q},\tau_z}|\Delta_{\boldsymbol{q},\tau_z}|^2 + \frac{\beta}{2}\left|\Delta_{\boldsymbol{q},\tau_z}\right|^4,\\
\alpha_{\boldsymbol{q},\tau_z} &= \alpha_0 + \gamma_{\tau_z}\boldsymbol{q}^2 + \kappa_{\tau_z}\left(q_x^3 - 3q_xq_y^2\right),\\
\alpha_0 &= \nu\frac{T-T_c}{T_c},\\
\gamma_{\tau_z} &= \frac{7\zeta(3)}{4}\frac{\nu\left(\tau_z\Delta_{\text{SOC}}^{(\ell)} - E_F\right)}{(\pi k_BT)^2}\frac{\hbar^2}{4m^*},\\
\kappa_{\tau_z} &= -\tau_z\nu\lambda_w\Delta_z\frac{93\zeta(5)}{16}\frac{\left(\tau_z\Delta_{\text{SOC}}^{(\ell)} - E_F\right)^2}{(\pi k_BT)^4},
\end{aligned} \tag{4}$$

where T is the temperature, ν is the density of states per spin and per valley, $\zeta(n)$ is the Riemann zeta function, and $\beta = 7\zeta(3)\nu/8(\pi k_BT)^2$. We minimize $\mathcal{F}[\Delta_{\boldsymbol{q},\tau_z}]$ with respect to $\Delta_{\boldsymbol{q},\tau_z}$ and the free energy becomes

$$F_{\boldsymbol{q},\tau_z} = -\alpha_{\boldsymbol{q},\tau_z}^2/(2\beta). \tag{5}$$

The supercurrent carried by the Cooper pairs with momentum $\boldsymbol{q}$ is calculated as

$$\boldsymbol{j} = \frac{2e}{\hbar}\sum_{\tau_z}\nabla_{\boldsymbol{q}}F_{\boldsymbol{q},\tau_z} = \frac{2e}{\hbar}\frac{1}{\beta}\sum_{\tau_z}|\alpha_{\boldsymbol{q},\tau_z}|\nabla_{\boldsymbol{q}}\alpha_{\boldsymbol{q},\tau_z}, \tag{6}$$

where $2e < 0$ is the charge of a Cooper pair, and therefore, $\boldsymbol{j}$ is antiparallel to $\boldsymbol{q}$. We parametrize $\boldsymbol{q}$ as $-q(\cos\theta, \sin\theta)$. The critical current is obtained by maximizing $|\boldsymbol{j}|$ with respect to q for $q > 0$, which leads to the following orientation dependence of the critical current:

$$j_c(\theta) = j_0(1 + \eta\cos 3\theta), \tag{7}$$

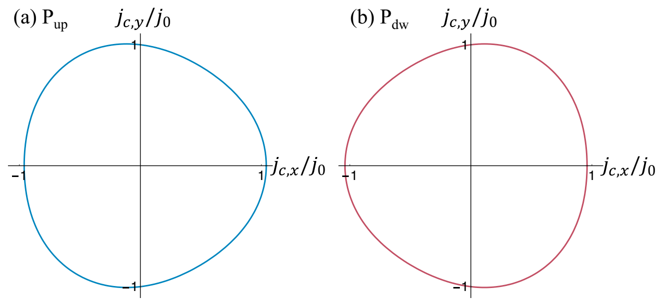

FIG. 4. The angle dependence of the critical current in (a) P_{up} state and (b) P_{dw} state. The nonreciprocal factor η is taken to be 0.04ℓ, where ℓ is $+1$ for P_{up} and -1 for P_{dw}, respectively.

where j_0 is the isotropic part of the critical current. In Eq. (7), the nonreciprocal factor η is given by

$$\begin{aligned}
\eta &= -\sqrt{\frac{|\alpha_0|}{3}}\frac{\sum_{\tau_z}\kappa_{\tau_z}/\gamma_{\tau_z}}{\sum_{\tau_z}\sqrt{\gamma_{\tau_z}}}\\
&\approx \sqrt{\frac{6}{7}}\frac{31\zeta(5)}{7\pi[\zeta(3)]^{3/2}}\frac{\lambda_w k_F^3\Delta_{\text{SOC}}^{(\ell)}}{|E_F|^2}\frac{\Delta_z}{k_BT}\sqrt{\frac{T_c-T}{T_c}}\\
&\approx 0.04\ell\frac{\Delta_z}{k_BT}\sqrt{\frac{T_c-T}{T_c}},
\end{aligned} \tag{8}$$

where k_F is defined as $\sqrt{2m^*|E_F|}/\hbar$. The factor η is proportional to $\Delta_{\text{SOC}}^{(\ell)}$, Δ_z and λ_w, which characterize, respectively, SOC-induced spin splittings due to inversion symmetry breaking, spin splittings due to time-reversal symmetry breaking, and trigonal warping. The critical current is generally different for opposite directions since $j_c(\theta) \neq j_c(\theta + \pi)$ for a generic θ, as shown in Fig. 4. We assume Δ_z is positive for definiteness in the following. In the P_{up} state, $\ell = +1$, which renders $\eta > 0$ and $j_c(0) > j_c(\pi)$; therefore, the system is superconducting for a current with a magnitude in the range of $j_0(1 - |\eta|, 1 + |\eta|)$ along $+\hat{x}$ direction, but resistive along the $-\hat{x}$ direction, which leads to the SDE. By contrast, $\ell = -1$ and $\eta < 0$ in the P_{dw} state; the superconducting direction is changed to the $-\hat{x}$ direction for a current with a magnitude in the same range. Therefore, the SDE is reversed upon ferroelectric reversal. As shown by Eq. (8), η increases with decreasing T. If we take $\Delta_z = k_BT = 0.1k_BT_c$, $\eta \approx 0.04\ell$, which represents an experimentally measurable effect [7].

Conclusions. In summary, we proposed a microscopic mechanism for ferroelectric reversible SDE using monolayer $CuNb_2Se_4$ as a model system. In addition to $CuNb_2Se_4$, we expect ferroelectricity can widely exist in 2D superconductors. In particular, sliding ferroelectricity has been shown to be ubiquitous in 2D vdW stacked layers, where the layer polarization can be switched by the in-plane interlayer sliding [21,58–63]. Thus, a superconducting vdW bilayer can naturally host coexisting superconductivity and ferroelectricity. A promising candidate is bilayer $MoTe_2$ in the T_d structure, which carries the sliding ferroelectricity and becomes superconducting at $T_c \sim 2$K [64]. The bilayer

$T_d - MoTe_2$ has Rashba spin splittings [65], and an in-plane magnetic field can effectively break the time-reversal symmetry. As in $CuNb_2Se_4$, ferroelectricity controls the sign of the Rashba spin splittings as well as the SDE in the bilayer $T_d - MoTe_2$. With the recent rapid developments in the study of 2D ferroelectric materials and nonreciprocal superconducting transport, we anticipate that our proposed ferroelectric reversible SDE should soon be experimentally realizable. In a broader prospective, our work establishes a new type of superconductor, in which ferroelectricity acts as a tuning knob in controlling the superconductivity properties. Further theoretical, computational, and experimental works are expected to substantially broaden the material candidates and device functionalities of ferroelectric superconductors.

Note added. Controlling of superconductivity through ferroelectricity was recently demonstrated in twisted bilayer graphene aligned with hBN [66].

Acknowledgments. This work is supported by National Key R&D Program of China (Grants No. 2018YFA0703700 and No. 2021YFA1401300), the National Natural Science Foundation of China (Grants No. 91964203, No. 62104171, No. 62104172, and No. 62004142), the Strategic Priority Research Program of Chinese Academy of Sciences (Grant No. XDB44000000), the Natural Science Foundation of Hubei Province, China (Grant No. 2021CFB037), and the Fundamental Research Funds for the Central Universities (Grant No. 2042021kf0067). The numerical calculations in this paper were done on the supercomputing system in the Supercomputing Center of Wuhan University.

[1] R. Wakatsuki, Y. Saito, S. Hoshino, Y. M. Itahashi, T. Ideue, M. Ezawa, Y. Iwasa, and N. Nagaosa, Nonreciprocal charge transport in noncentrosymmetric superconductors, Sci. Adv. **3**, e1602390 (2017).

[2] F. Qin, W. Shi, T. Ideue, M. Yoshida, A. Zak, R. Tenne, T. Kikitsu, D. Inoue, D. Hashizume, and Y. Iwasa, Superconductivity in a chiral nanotube, Nat. Commun. **8**, 14465 (2017).

[3] R. Wakatsuki and N. Nagaosa, Nonreciprocal Current in Noncentrosymmetric Rashba Superconductors, Phys. Rev. Lett. **121**, 026601 (2018).

[4] S. Hoshino, R. Wakatsuki, K. Hamamoto, and N. Nagaosa, Nonreciprocal charge transport in two-dimensional noncentrosymmetric superconductors, Phys. Rev. B **98**, 054510 (2018).

[5] J. Lustikova, Y. Shiomi, N. Yokoi, N. Kabeya, N. Kimura, K. Ienaga, S. Kaneko, S. Okuma, S. Takahashi, and E. Saitoh, Vortex rectenna powered by environmental fluctuations, Nat. Commun. **9**, 4922 (2018).

[6] K. Yasuda, H. Yasuda, T. Liang, R. Yoshimi, A. Tsukazaki, K. S. Takahashi, N. Nagaosa, M. Kawasaki, and Y. Tokura, Nonreciprocal charge transport at topological insulator/superconductor interface, Nat. Commun. **10**, 2734 (2019).

[7] F. Ando, Y. Miyasaka, T. Li, J. Ishizuka, T. Arakawa, Y. Shiota, T. Moriyama, Y. Yanase, and T. Ono, Observation of superconducting diode effect, Nature (London) **584**, 373 (2020).

[8] Y.-Y. Lyu, J. Jiang, Y.-L. Wang, Z.-L. Xiao, S. Dong, Q.-H. Chen, M. V. Milošević, H. Wang, R. Divan, J. E. Pearson, P. Wu, F. M. Peeters, and W.-K. Kwok, Superconducting diode effect via conformal-mapped nanoholes, Nat. Commun. **12**, 2703 (2021).

[9] C. Baumgartner, L. Fuchs, A. Costa, S. Reinhardt, S. Gronin, G. C. Gardner, T. Lindemann, M. J. Manfra, P. E. Faria Junior, D. Kochan, J. Fabian, N. Paradiso, and C. Strunk, Supercurrent rectification and magnetochiral effects in symmetric Josephson junctions, Nat. Nanotechnol. **17**, 39 (2021).

[10] H. Wu, Y. Wang, Y. Xu, P. K. Sivakumar, C. Pasco, U. Filippozzi, S. S. P. Parkin, Y.-J. Zeng, T. McQueen, and M. N. Ali, The field-free Josephson diode in a van der Waals heterostructure, Nature (London) **604**, 653 (2022).

[11] L. Bauriedl, C. Bäuml, L. Fuchs, C. Baumgartner, N. Paulik, J. M. Bauer, K.-Q. Lin, J. M. Lupton, T. Taniguchi, K. Watanabe, C. Strunk, and N. Paradiso, Supercurrent diode effect and magnetochiral anisotropy in few-layer $NbSe_2$, Nat. Commun. **13**, 4266 (2022).

[12] J. Shin, S. Son, J. Yun, G. Park, K. Zhang, Y. J. Shin, J.-G. Park, and D. Kim, Magnetic proximity-induced superconducting diode effect and infinite magnetoresistance in van der waals heterostructure, arXiv:2111.05627.

[13] J.-X. Lin, P. Siriviboon, H. D. Scammell, S. Liu, D. Rhodes, K. Watanabe, T. Taniguchi, J. Hone, M. S. Scheurer, and J. Li, Zero-field superconducting diode effect in small-twist-angle trilayer graphene, Nat. Phys. **18**, 1221 (2022).

[14] N. F. Q. Yuan and L. Fu, Supercurrent diode effect and finite-momentum superconductors, Proc. Natl. Acad. Sci. USA **119**, e2119548119 (2022).

[15] A. Daido, Y. Ikeda, and Y. Yanase, Intrinsic Superconducting Diode Effect, Phys. Rev. Lett. **128**, 037001 (2022).

[16] J. J. He, Y. Tanaka, and N. Nagaosa, A phenomenological theory of superconductor diodes, New J. Phys. **24**, 053014 (2022).

[17] H. D. Scammell, J. I. A. Li, and M. S. Scheurer, Theory of zero-field superconducting diode effect in twisted trilayer graphene, 2D Mater. **9**, 025027 (2022).

[18] K. Halterman, M. Alidoust, R. Smith, and S. Starr, Supercurrent diode effect, spin torques, and robust zero-energy peak in planar half-metallic trilayers, Phys. Rev. B **105**, 104508 (2022).

[19] J.-X. Lin, P. Siriviboon, H. D. Scammell, S. Liu, D. Rhodes, K. Watanabe, T. Taniguchi, J. Hone, M. S. Scheurer, and J. Li, Zero-field superconducting diode effect in twisted trilayer graphene, arXiv:2112.07841.

[20] Z. Fei, W. Zhao, T. A. Palomaki, B. Sun, M. K. Miller, Z. Zhao, J. Yan, X. Xu, and D. H. Cobden, Ferroelectric switching of a two-dimensional metal, Nature (London) **560**, 336 (2018).

[21] M. Wu and J. Li, Sliding ferroelectricity in 2D van der Waals materials: Related physics and future opportunities, Proc. Natl. Acad. Sci. USA **118**, e2115703118 (2021).

[22] R. B. Somoano and A. Rembaum, Superconductivity in Intercalated Molybdenum Disulfide, Phys. Rev. Lett. **27**, 402 (1971).

[23] K. Anzenhofer, J. M. V. D. Berg, P. Cossee, and J. N. Helle, The crystal structure and magnetic susceptibilities of $MnNb_3S_6$, $FeNb_3S_6$, $CoNb_3S_6$ and $NiNb_3S_6$, J. Phys. Chem. Solids **31**, 1057 (1970).

[24] S. S. P. Parkin, E. A. Marseglia, and P. J. Brown, Magnetic structure of $Co_{1/3}NbS_2$ and $Co_{1/3}TaS_2$, J. Phys. C: Solid State Phys. **16**, 2765 (1983).

[25] N. J. Ghimire, A. S. Botana, J. S. Jiang, J. Zhang, Y.-S. Chen, and J. F. Mitchell, Large anomalous Hall effect in the chiral-lattice antiferromagnet $CoNb_3S_6$, Nat. Commun. **9**, 3280 (2018).

[26] G. Tenasini, E. Martino, N. Ubrig, N. J. Ghimire, H. Berger, O. Zaharko, F. Wu, J. F. Mitchell, I. Martin, L. Forró, and A. F. Morpurgo, Giant anomalous Hall effect in quasi-two-dimensional layered antiferromagnet $Co_{1/3}NbS_2$, Phys. Rev. Res. **2**, 023051 (2020).

[27] S.-L. Yang, J. A. Sobota, C. A. Howard, C. J. Pickard, M. Hashimoto, D. H. Lu, S.-K. Mo, P. S. Kirchmann, and Z.-X. Shen, Superconducting graphene sheets in CaC_6 enabled by phonon-mediated interband interactions, Nat. Commun. **5**, 3493 (2014).

[28] E. R. Margine, H. Lambert, and F. Giustino, Electron-phonon interaction and pairing mechanism in superconducting Ca-intercalated bilayer graphene, Sci. Rep. **6**, 21414 (2016).

[29] Z. Tu and M. Wu, 2D Diluted Multiferroic Semiconductors upon Intercalation, Adv. Electron. Mater. **5**, 1800960 (2019).

[30] K. Kanetani, K. Sugawara, T. Sato, R. Shimizu, K. Iwaya, T. Hitosugi, and T. Takahashi, Ca intercalated bilayer graphene as a thinnest limit of superconducting C_6Ca, Proc. Natl. Acad. Sci. USA **109**, 19610 (2012).

[31] S. Ichinokura, K. Sugawara, A. Takayama, T. Takahashi, and S. Hasegawa, Superconducting calcium-intercalated bilayer graphene, ACS Nano **10**, 2761 (2016).

[32] K. Ji, J. Han, A. Hirata, T. Fujita, Y. Shen, S. Ning, P. Liu, H. Kashani, Y. Tian, Y. Ito, J.-i. Fujita, and Y. Oyama, Lithium intercalation into bilayer graphene, Nat. Commun. **10**, 275 (2019).

[33] X. Xi, Z. Wang, W. Zhao, J.-H. Park, K. T. Law, H. Berger, L. Forró, J. Shan, and K. F. Mak, Ising pairing in superconducting $NbSe_2$ atomic layers, Nat. Phys. **12**, 139 (2016).

[34] G. Kresse and J. Furthmüller, Efficiency of ab-initio total energy calculations for metals and semiconductors using a plane-wave basis set, Comput. Mater. Sci. **6**, 15 (1996).

[35] See Supplemental Material at http://link.aps.org/supplemental/10.1103/PhysRevB.106.L140505 for first-principles computational methods and derivation of the free energy for superconductivity.

[36] J. P. Perdew, K. Burke, and M. Ernzerhof, Generalized Gradient Approximation Made Simple, Phys. Rev. Lett. **77**, 3865 (1996).

[37] P. E. Blöchl, Projector augmented-wave method, Phys. Rev. B **50**, 17953 (1994).

[38] H. J. Monkhorst and J. D. Pack, Special points for brillouin-zone integrations, Phys. Rev. B **13**, 5188 (1976).

[39] T. Sohier, M. Calandra, and F. Mauri, Density functional perturbation theory for gated two-dimensional heterostructures: Theoretical developments and application to flexural phonons in graphene, Phys. Rev. B **96**, 075448 (2017).

[40] A. Togo and I. Tanaka, First principles phonon calculations in materials science, Scr. Mater. **108**, 1 (2015).

[41] G. Henkelman, A. Arnaldsson, and H. Jónsson, A fast and robust algorithm for Bader decomposition of charge density, Comput. Mater. Sci. **36**, 354 (2006).

[42] G. Henkelman, B. P. Uberuaga, and H. Jónsson, A climbing image nudged elastic band method for finding saddle points and minimum energy paths, J. Chem. Phys. **113**, 9901 (2000).

[43] W. Ding, J. Zhu, Z. Wang, Y. Gao, D. Xiao, Y. Gu, Z. Zhang, and W. Zhu, Prediction of intrinsic two-dimensional ferroelectrics in In_2Se_3 and other III_2-VI_3 van der Waals materials, Nat. Commun. **8**, 14956 (2017).

[44] D. Xiao, G.-B. Liu, W. Feng, X. Xu, and W. Yao, Coupled Spin and Valley Physics in Monolayers of MoS_2 and Other Group-VI Dichalcogenides, Phys. Rev. Lett. **108**, 196802 (2012).

[45] X.-C. Liu, S. Zhao, X. Sun, L. Deng, X. Zou, Y. Hu, Y.-X. Wang, C.-W. Chu, J. Li, J. Wu, F.-S. Ke, and P. M. Ajayan, Spontaneous self-intercalation of copper atoms into transition metal dichalcogenides, Sci. Adv. **6**, eaay4092 (2020).

[46] H. Luo, J. Strychalska-Nowak, J. Li, J. Tao, T. Klimczuk, and R. J. Cava, S-shaped suppression of the superconducting transition temperature in Cu-intercalated $NbSe_2$, Chem. Mater. **29**, 3704 (2017).

[47] W. L. McMillan, Transition temperature of strong-coupled superconductors, Phys. Rev. **167**, 331 (1968).

[48] P. B. Allen and R. C. Dynes, Transition temperature of strong-coupled superconductors reanalyzed, Phys. Rev. B **12**, 905 (1975).

[49] F. Giustino, Electron-phonon interactions from first principles, Rev. Mod. Phys. **89**, 015003 (2017).

[50] P. Giannozzi, S. Baroni, N. Bonini, M. Calandra, R. Car, C. Cavazzoni, D. Ceresoli, G. L. Chiarotti, M. Cococcioni, I. Dabo, A. Dal Corso, S. de Gironcoli, S. Fabris, G. Fratesi, R. Gebauer, U. Gerstmann, C. Gougoussis, A. Kokalj, M. Lazzeri, L. Martin-Samos *et al.*, QUANTUM ESPRESSO: a modular and open-source software project for quantum simulations of materials, J. Phys.: Condens. Matter **21**, 395502 (2009).

[51] J. Noffsinger, F. Giustino, B. D. Malone, C.-H. Park, S. G. Louie, and M. L. Cohen, EPW: A program for calculating the electron-phonon coupling using maximally localized Wannier functions, Comput. Phys. Commun. **181**, 2140 (2010).

[52] S. Poncé, E. R. Margine, C. Verdi, and F. Giustino, EPW: Electron-phonon coupling, transport and superconducting properties using maximally localized Wannier functions, Comput. Phys. Commun. **209**, 116 (2016).

[53] X. Xi, H. Berger, L. Forró, J. Shan, and K. F. Mak, Gate Tuning of Electronic Phase Transitions in Two-Dimensional $NbSe_2$, Phys. Rev. Lett. **117**, 106801 (2016).

[54] J. Qi, X. Li, Q. Niu, and J. Feng, Giant and tunable valley degeneracy splitting in $MoTe_2$, Phys. Rev. B **92**, 121403(R) (2015).

[55] S. Kezilebieke, M. N. Huda, V. Vaňo, M. Aapro, S. C. Ganguli, O. J. Silveira, S. Głodzik, A. S. Foster, T. Ojanen, and P. Liljeroth, Topological superconductivity in a van der Waals heterostructure, Nature (London) **588**, 424 (2020).

[56] H. Narita, J. Ishizuka, R. Kawarazaki, D. Kan, Y. Shiota, T. Moriyama, Y. Shimakawa, A. V. Ognev, A. S. Samardak, Y. Yanase, and T. Ono, Field-free superconducting diode effect in noncentrosymmetric superconductor/ferromagnet multilayers, Nat. Nanotechnol. **17**, 823 (2022).

[57] Y. Zhang, Y. Gu, P. Li, J. Hu, and K. Jiang, General theory of Josephson Diodes, arXiv:2112.08901.

[58] M. Wu and X. C. Zeng, Intrinsic ferroelasticity and/or multiferroicity in two-dimensional phosphorene and phosphorene analogues, Nano Lett. **16**, 3236 (2016).

[59] L. Li and M. Wu, Binary compound bilayer and multilayer with vertical polarizations: Two-dimensional ferroelectrics, multiferroics, and nanogenerators, ACS Nano **11**, 6382 (2017).

[60] Q. Yang, M. Wu, and J. Li, Origin of two-dimensional vertical ferroelectricity in WTe_2 bilayer and multilayer, J. Phys. Chem. Lett. **9**, 7160 (2018).

[61] K. Yasuda, X. Wang, K. Watanabe, T. Taniguchi, and P. Jarillo-Herrero, Stacking-engineered ferroelectricity in bilayer boron nitride, Science **372**, 1458 (2021).

[62] M. Vizner Stern, Y. Waschitz, W. Cao, I. Nevo, K. Watanabe, T. Taniguchi, E. Sela, M. Urbakh, O. Hod, and M. Ben Shalom, Interfacial ferroelectricity by van der Waals sliding, Science **372**, 1462 (2021).

[63] X. Wang, K. Yasuda, Y. Zhang, S. Liu, K. Watanabe, T. Taniguchi, J. Hone, L. Fu, and P. Jarillo-Herrero, Interfacial ferroelectricity in rhombohedral-stacked bilayer transition metal dichalcogenides, Nat. Nanotechnol. **17**, 367 (2022).

[64] D. A. Rhodes, A. Jindal, N. F. Q. Yuan, Y. Jung, A. Antony, H. Wang, B. Kim, Y.-c. Chiu, T. Taniguchi, K. Watanabe, K. Barmak, L. Balicas, C. R. Dean, X. Qian, L. Fu, A. N. Pasupathy, and J. Hone, Enhanced superconductivity in monolayer T_d-$MoTe_2$, Nano Lett. **21**, 2505 (2021).

[65] J. Cui, P. Li, J. Zhou, W.-Y. He, X. Huang, J. Yi, J. Fan, Z. Ji, X. Jing, F. Qu, Z. G. Cheng, C. Yang, L. Lu, K. Suenaga, J. Liu, K. T. Law, J. Lin, Z. Liu, and G. Liu, Transport evidence of asymmetric spin-orbit coupling in few-layer superconducting $1T_d$-$MoTe_2$, Nat. Commun. **10**, 2044 (2019).

[66] D. R. Klein, L.-Q. Xia, D. MacNeill, K. Watanabe, T. Taniguchi, and P. Jarillo-Herrero, Electrical switching of a moiré ferroelectric superconductor, arXiv:2205.04458.